Materials & Design 224 (2022) 111335

Contents lists available at ScienceDirect

Materials & Design

journal homepage: www.elsevier.com/locate/matdes

Kirigami inspired shape programmable and reconfigurable multifunctional nanocomposites for 3D structures

Arnaud Kernin [a], Leonardo Ventura [a], Aaron Soul [a], Kan Chen [a], Kening Wan [a], Weibang Lu [b], Pietro Steiner [c,d], Coskun Kocabas [c,d], Dimitrios Papageorgiou [a], Stergios Goutianos [e], Han Zhang [a], Emiliano Bilotti [a,f,*]

[a] School of Engineering and Materials Science, Queen Mary University of London, London, Great Britain and Northern Ireland, UK
[b] Division of Advanced Nanomaterials and Innovation Center for Advanced Nanocomposites, Suzhou Institute of Nano-Tech and Nano-Bionics, Chinese Academy of Sciences, Suzhou 215123, China
[c] Department of Materials, University of Manchester, Manchester, Great Britain and Northern Ireland, UK
[d] National Graphene Institute, University of Manchester, Manchester, Great Britain and Northern Ireland, UK
[e] Department of Manufacturing and Civil Engineering, Norwegian University of Science and Technology, 2815 Gjøvik, Norway
[f] Department of Aeronautics, Imperial College London, South Kensington Campus, SW7 2AZ London, UK

HIGHLIGHTS

- The kirigami design strategy can achieve a controlled sequential folded honeycomb structure by combining different patterns of hinges.
- The sequential self-folding approach allows to accurately position nanoparticles in 3D space and time and, hence, controlling properties and anisotropies.
- The multifunctional self-folded honeycomb can go beyond the typical sensing/actuation dichotomy with capabilities to both actuate and sense.

GRAPHICAL ABSTRACT

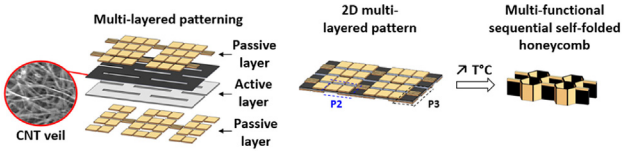

ARTICLE INFO

Article history:
Received 12 June 2022
Revised 21 October 2022
Accepted 28 October 2022
Available online 29 October 2022

Keywords:
3D shape-programming
Multifunctional composite
carbon nanotubes
Origami/Kirigami
Shape-memory polymer
sequential folding
sensing
actuation

ABSTRACT

The ability to shape and program remotely and contactlessly from two-dimensional (2D) flat multilayer materials into three-dimensional (3D) structures and functional devices could be ideal for applications like space missions, environmental remediation and minimally invasive surgery. However, achieving a fast and accurate deployment of complex 3D shapes contactlessly at low energy consumption, while embedding a number of physical properties and functionalities, remains very challenging. Herein, a strategy to widen the complexity space of 3D shapes and functions achievable is demonstrated, by enabling a controlled sequential folding while incorporating nano-reinforcements. Sequential folding was successfully achieved and a honeycomb structure was developed by designing multilayer polymer films with different kirigami patterns - each responding at a different rate upon heating. A finite element method (FEM) model was developed to better understand the main underlying physical mechanism as well as to feedback into materials and structure design. Moreover, a shape-programmed CNT veil-based honeycomb structure was developed, triggered remotely by thermal stimuli, with capability to self-sense the folding state through the electrical resistance change ($\Delta R/R_0$ = 100–300 %). Overall, it was demonstrated that designing layered nanocomposites with different 2D patterns allows an accurate sequential folding into 3D structures, with bespoke physical properties and integrated sensing–actuating functionalities.

* Corresponding author at: Department of Aeronautics, Imperial College London, South Kensington Campus, SW7 2AZ London, UK.
E-mail address: e.bilotti@imperial.ac.uk (E. Bilotti).

https://doi.org/10.1016/j.matdes.2022.111335
0264-1275/

1. Introduction

Over the past decade, two-dimensional (2D) programmable materials have attracted a great interest by their capability to self-transform their flat shape into a complex three-dimensional (3D) geometry in response to external stimuli. 3D shape programming of polymeric materials is particularly compelling because of the potential of using biocompatible, flexible, durable, low-cost, and lightweight polymers, in fields such as minimally invasive surgeries [1], soft robotics [2], environmental remediation [3] and space exploration [4].

Promising 3D shape programming of polymer materials has been achieved through several approaches, such as shape memory polymers (SMP) [5,6], swelling hydrogels [7,8], or liquid crystalline elastomers (LCE) [9,10]. Different bending strategies have been used, including multilayers [11], material gradients [12] and localized activation [13]. In opposition to the bending strategy, where the gradient in properties (or stress gradient during actuation) is in the out-of-plane of the material layer (namely through the thickness), buckling requires an in-plane gradient. Different buckling strategies have been used to induce 3D programming, such as material tessellation [14], in-plane material gradients [15], non-homogenous exposure [16] and mechanically induced buckling [17]. These methods confer a strong knowledge on the shape morphing mechanisms but do not allow to develop shapes complex enough for certain engineering applications.

In order to overcome the shape limitations, the ancient Japanese art of origami and kirigami offers a great inspiration to obtain a large variety of 3D shapes from simply folding/buckling and/or cutting a 2D sheet of paper, since the geometrical design is a critical factor for shape-shifting 2D sheets into desired 3D structures. Self-folding of origami-engineered structures allows a large number of possibilities, promising high-speed actuation [18], high strength-to-weight ratios [19], size independency from meters to nanometers [20], with relatively low processing time and energy.

However, achieving a fast and accurate deployment of complex 3D shapes, at low energy and contactlessly, while embedding a number of physical properties, such as mechanical, electrical, thermal, and functionalities such as sensing and actuating, remains very challenging.

Incorporating electrical resistors in self-folding structures can help producing active hinges for automatic fabrication and robotics [2]; however, the process is limited to achieving only actuation without adding any other functionality to the structure. Self-folding of origami shape memory polymer patterns has been programmed into various configurations using Joule heating by incorporating heating elements such as printed copper circuit [2], printed graphene ink [21], graphene network [22].

Graphene oxide papers have been programmed to fold and unfold in response to heating or light irradiation using through-the-thickness gradients [23].

Transparent 3D curvilinear self-folding glassy polymer structures have also been developed using selective light absorption to actuate the shape [24]. Conductive materials have been casted and patterned onto a polymer film in order to achieve multifunctionalities such as optical transparency and electrical conductivity.

Herein, a strategy to widen the complexity space of 3D programmed shapes and functions achievable is demonstrated, by enabling a controlled sequential folding during actuation while incorporating nanoparticles (i.e., carbon nanotubes (CNT) veils) into the structure. Sequential folding into complex 3D shapes is achieved by designing and combining three simple actuating multilayer units formed by constraining passive layers onto an oriented polymer film. Upon heating above its glass transition temperature (Tg), the oriented polymer shrinks non-uniformly, which leads to inhomogeneous strain relaxation, a bending actuation with unique and well-defined kinematics and, hence, sequential folding.

To validate the experimental data, with the aim of creating a universal strategy for this field, a finite element method (FEM) model has been developed to better understand the underlying physical mechanism during actuation, as well as to feedback into material properties, geometrical features, structure design and different arrangements of the passive and active polymers.

With the aim to go beyond geometrical 3D shape programming per se and to obtain unique physical properties and functionalities, a self-folding CNT veil-based honeycomb structure, inspired by the Japanese art of kirigami, was also developed. By using the versatility offered by origami and kirigami, this multi-layered honeycomb pattern allows to drive the positioning of nanoparticles (hence high electrical and thermal conductivity) from, initially, in the in-plane directions to the out-of-plane direction once actuated. Moreover, it is demonstrated that this system can go beyond the typical sensing/actuation dichotomy with capabilities to both actuate and sense.

2. Experimental

2.1. Materials

Pre-strained polystyrene (PS) heat shrinkable films, with a thickness of 300 μm (±5μm), were supplied by Grafix Shrink Film and used as received. These pre-strained polymer films shrink in-plane while heating over the transition temperature (∼105 °C). Bondit cyanoacrylate adhesive (code product: HUC1620) was used to glue paperboard (Canson 200 g/m^2) on the polymer films.

2.2. CNT veils fabrication

CNT veils were made using the floating catalyst chemical vapor deposition (FCCVD) method. A solution containing 96.5 wt% ethanol (carbon source), 1.9 wt% ferrocene (catalyst precursor) and 1.6 wt% thiophene (promoter), was injected (0.15 ml/min) into a hot CVD furnace (∼1150 °C) along with the carrier gas (600 ml/min) consisting of hydrogen and argon (ca. 1:1 volume), according to previous reported methods [25]. CNTs were formed and entangled into sock-like aerogel in the furnace, then was pulled out and collected by a rotating roller continuously. As a result, the high porosity CNT sponge on the roller was half densified by mechanical compression and followed by the annealing-acid wash procedure.

2.3. Composite preparation

Three patterns were designed, named Pattern 1, 2 and 3. The dimensions of Patterns 1 and 2 were 21 mm (length) × 10 mm (width), in which the paperboards were cut into squares of dimension 10 mm × 10 mm using a Silhouette Cameo. Pattern 1 has two squares glued on the PS films leaving a hinge of 1 mm in the middle. Pattern 2 has three squares glued on the PS films, the third one is glued on the bottom side under one of the two previous glued square. The dimensions of Pattern 3 were 28 mm (length) × 10 mm (width), in which two paperboards were cut into squares with a dimension of 10 mm × 10 mm then glued on the same side of the polymer film leaving a gap of 8 mm. Two rectangular paperboards of dimension 2 mm × 10 mm are glued on the other side than the two previous ones with a gap of 1 mm between them.

PS films and CNT veils were cut into the designed honeycomb pattern. Three types of the paperboard patches have been cut by Silhouette Cameo: the first patche with a dimension of 14 mm × 10 mm, the second with a dimension of 12 mm × 10 mm and the third with a dimension of 2 mm × 10 mm. All the patches have been glued on the PS/CNTs veil patterns following the honeycomb pattern. The as-assembled samples were put in the oven at a temperature of 140 °C, for self-folding experiments. The temperature has been measured on top of the specimens using a Proster digital thermocouple with a Dual K-Type Channel temperature sensor. At least 10 specimens were tested for each pattern to obtain a good repeatability of the results and an average value has been calculated. A CNTs veil has been added to the Patterns 1, 2 and 3 and actuated using a power supply.

3. Characterization

3.1. Dynamic mechanical analysis (DMA)

Thermal shrinkage percentage and maximum thermal shrinkage stress measurements were performed with a DMA Q800 from TA Instruments, equipped with the tensile mode clamps, for PS. The distance between the clamps was 10 mm, and the width of the polymer samples was around 3 mm. Controlled-force mode was used to measure the thermal shrinkage percentage and the thermal expansion coefficient of each film with a pre-load force of 0.01 N. Isostrain mode was used to measure the maximum thermal shrinkage stress with a strain of 0.0075 % and a pre-load force of 0.0075 N. For each mode, measurements were performed from room temperature to 180 °C at a heating rate of 10 °C/min.

3.2. Tensile testing

Tensile tests were performed on different bi-oriented polymer films, according to ASTM D638-10 and D882-02, on an Instron 5566 universal tensile testing machine, equipped with a 1 kN load cell. Rectangular sample strips, 185 mm long, were cut along chosen directions (0°, 90° and 45°), for each polymer film, and tested at a crosshead speed of 12.5 mm/min. The Young's Modulus of each specimen is calculated as the gradient of the stress vs strain curve between 0.1 % and 0.4 % strain, which is approximately linear for all the films. At least 5 specimens were tested for each polymer film and each direction, and average values reported.

3.3. Self-folding sensing

Electrical resistance sensing performance was characterized by monitoring the electrical resistance variation before folding and upon folding of the specimens. The electrodes were attached to the surface of the specimen directly from the ends of the specimens by connecting copper wires with silver paint. A constant voltage was applied throughout the test.

The folding angle change with time were recorded by videos on the side views of the samples in an oven at 140 °C, and analysis by Image J software.

3.4. Electrical conductivity

A bespoke four-point probe system consisting of an Agilent 6614 System DC power supply, a Keithley 6485 picoammeter and a Keithley 2000 multimeter, was used for in-plane electrical conductivity of the CNT veils with a probe space of 2.5 mm. The thickness of the CNT veils was measured by Bruker Dektak Vision 64 profilometer. 10 specimens were tested and average values reported.

3.5. Thermal conductivity

The in-plane thermal diffusivities of the CNT veils were measured using a bespoke setup consisting of a pulsed (1 Hz) tunable laser beam to excite heat waves that propagates periodically into the sample and a high-resolution infrared camera (FLIR T660) as detector. The camera was mounted with an IR micro lens (pixel size 50 × 50). Thermal diffusivity was determined following the Angstrom method. Thermal conductivity (κ) was then calculated using the equation below,

$$k\cdot = \cdot\lambda \cdot c_p \cdot d$$

where λ is the thermal diffusivity, c_p is the specific heat capacity and d is density.

4. Results and discussions

4.1. Sequential folding using multilayer strategy to achieve complex structures

A controlled sequential folding was achieved by designing and combining three simple actuating units (also referred to as patterns). Each unit is formed by passive rigid layers of paperboard glued onto an active shrinking layer made of a bi-axially oriented polystyrene (BOPS) film (Fig. 1a). In the gaps (acting as hinges) between passive constrain layers, the active layer deforms as the temperature increases generating a bending moment and allowing the multilayer unit to fold.

The three patterns, denoted as *P*1, *P*2 and *P*3, are shown in Fig. 1a. The first pattern, *P*1, is constituted by two structural passive layers glued on one side of the polymer films and separated by a hinge with length equal to 1 mm in the middle. The second pattern, *P*2, is the same as the first one but with an additional passive layer glued also on the bottom side of one end of the oriented PS. The last pattern, *P*3, is a set of two hinges of 1 mm, separated with three passive layers 2 mm long and two additional passive layers on the other side of the PS film.

Fig. 1b-c shows the folding angle of the three different patterns as a function of time, when the temperature is ramped up to 140 °C (heating curve in Fig. 1b bottom).

For all three patterns, after an initial slight opening (anticlockwise rotation) of the hinge of up to −5° within 10 to 40 s (stage I), the hinge rather rapidly closes within 30 s (clockwise rotation), until reaching a maximum point (stage II).

The movements during the first two stages are attributed to the thermo-mechanical response of BOPS films (Figure S1a, SI). Upon increasing of temperature, the BOPS layer first slightly expands by 0.1 % and then contracts up to a max of 50.5 %. This is a typical behaviour of oriented polymer films [26], confirmed by stress relaxation and creep tests (Figure S1b, SI). At temperatures only slightly above the glass transition temperature and for short period of time (Stage I), thermal activation cannot be accompanied by extensive dimensional changes [26]. The release of local stresses in the recently activated molecular chains causes the relaxation, leading to intermolecular slipping. Due to a combination of the relaxation of the chains, and the film being constrained by the passive layer, the resulting bending is in the anti-clockwise direction (i.e. the hinge opens).

At higher temperatures, and/or for longer times, the dominant phenomenon is a localised contraction (negative thermal expansion) in the hinge region, where the BOPS is unconstrained (Stage II). Negative thermal expansions in oriented amorphous polymers

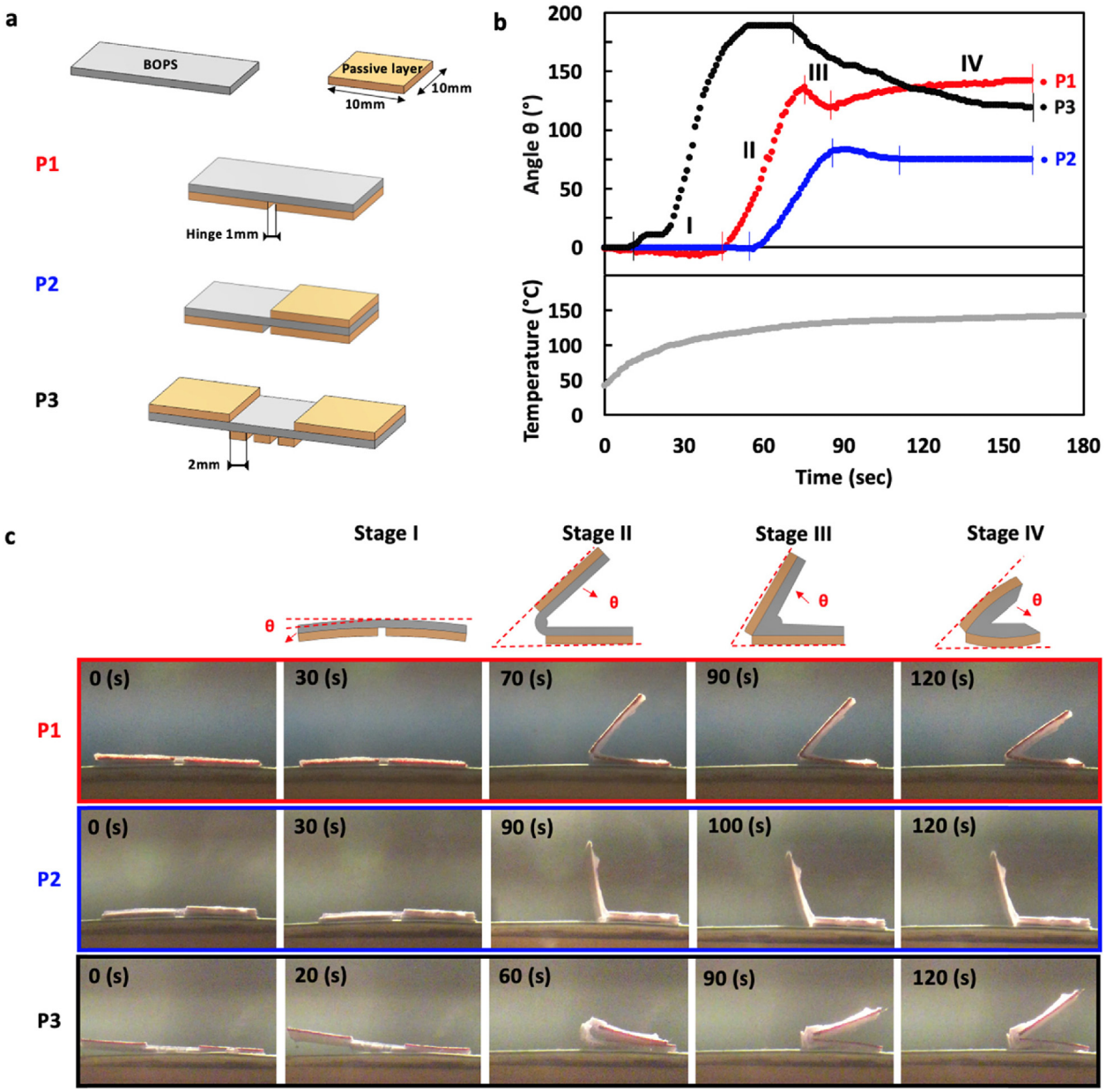

Fig. 1. Effect of different patterned multi-layered films on the self-folding speed and the self-folding angles. (a) Schematic illustration of three multi-layered patterns with different hinges and layered composition, namely *P*1, *P*2 and *P*3, composed of an active layer (a BOPS film) and a passive layer (paperboard). (b) Self-folding angles of *P*1, *P*2 and *P*3 as a function of time: the folding of each pattern develops along four distinct stages (top), in correspondence of the same temperature profile (bottom). (c) Images of *P*1, *P*2 and *P*3 while self-folding.

can be explained by the entropic spring effect [26,27]. The draw ratio of our BOPS - determined by tensile tests (Figure S2a-b, SI) - is about two, hence the film contracts by about 45, 55, 51 % respectively for 0° (extrusion direction), 90° and 45° orientation. At the end of Stage II, the polymer film located at the hinge is fully relaxed and forms a 'bulk' mass (about 0.75 mm thick). The localized contraction exerts a bending moment of the hinge allowing the sample to fold until a maximum angle is reached. It is interesting to notice that during Stage II each pattern reaches a different maximum closing angle at different times; Patterns 1, 2 and 3 reach a maximum angle of 137°, 80° and 190°, after 75 s, 85 s and 50 s, respectively.

The smaller angle of *P*2 in comparison with *P*1 can be explained by the presence of two passive layers at the top and the other at bottom of the BOPS films, which exert a stronger constraint effect on one side of the active polymer film. *P*3 achieves a higher folding angle (180°) at a faster speed compared to *P*1 and *P*2, which can be attributed to the presence of two hinges at a distance 1 mm apart.

The first two stages of *P*1, *P*2 and *P*3 have been exploited within this work to achieve control over the folding sequence, hence widening the spectrum to more complex and better folding-controlled structures (Fig. 4).

However, the three patterns undergo further changes if left for even longer periods of time at high temperature (140 °C). In particular, a decrease in the closing angle is normally witnessed after the maximum point (Stage III). For instance, the opening angle of *P*1 slightly decreases from 137° to 120°. During Stage III the polymer film, away from the hinge and in contact with the constraint layer,

begins to relax leading to a shrinkage gradient along the in-plane and through-the-thickness directions. Ultimately, the angle decreases because more polymer is pulled from the constrained region into the hinge region, which in turn causes the internal ends of the constraint layers to get closer to each other and the hinge to rotate anticlockwise about the bulk mass (Fig. 1c).

In Stage IV, the relaxation of the BOPS film manifests itself even deeper in the constrained regions and further away from the hinge, augmenting the shrinkage gradients along the in-plane and through-the-thickness directions. This causes two main effects: i) the 'bulk' mass propagates away from hinge, pulling the two free ends of the constraint layers closer to each other and ii) the constraint layers bend generating a Gaussian curvature (Fig. 1c).

These two effects result in an overall increase of the angle in the case of *P*1 and *P*2 but a decrease of the angle in the case of *P*3. This opposite effect is explained by the relative position of the hinges and the passive constraint layer, which, in the case of *P*1 and *P*2 is on the same side of the BOPS, while, in the case of *P*3, is on opposite sides.

In conclusion of this section, a method to control folding angle over a wide range (from 0° to more than 180°) and speed, has been demonstrated, by just exploiting the thermomechanical response of oriented polymer films in different multilayer configurations (*P*1, *P*2 and *P*3). In this study, the relatively short response time features of Stage I and II is used. But the more intricate response discovered over longer period of times (Stage III and IV) could be exploited in the future. In particular, the possibility to partially reverse the actuation motion (i.e. rotation) in correspondence of a single and invariant stimulus (i.e. environmental temperature) is unique in the literature. For instance, tuning parameters like the draw ratio and the thickness of the oriented active layer, hence the longitudinal and transverse stress gradient within the constrained region could provide additional design degree of freedom for more complex structures and functions.

4.2. FEM modelling

The self-folding behaviour was modelled in two steps using the Abaqus commercial finite element software as a two-dimensional problem (Fig. 2). The first step (Fig. 2a) consisted of a transient heat transfer analysis to calculate the temperature in the self-folding structure as a function of time, given a certain external temperature. Then, the external temperature as a function of time (experimental input, (Figure S3, SI)) was applied to the mechanical dynamic model shown in Fig. 2b to predict the self-folding response.

By using this modelling framework, the opening angle of all three patterns can be well reproduced (Fig. 3.a-c) after exposure to the same temperature profile as in the experiments (Fig. 1b (bottom)), and after inputting the thermo-mechanical behaviour of the active PS film (Figure S3, SI). In fact, the model is able to predict the entire folding kinematic of Stage I and II (Fig. 2c). The model does not currently include viscoelastic behaviour necessary to predict also Stage III and IV.

4.3. Sequential folding for more complex 3D shapes

Now that the mechanism of actuation and its control is better understood, one simple honeycomb structure demonstrator is reported that highlight the importance of sequential folding in accessing 3D shapes and functions (Fig. 4).

The self-folding honeycomb structure, inspired by kirigami, has been successfully developed, initially composed of flat thin sheet panels that are interconnected by hinges (fold lines) (Fig. 4a) and actuated through temperature change. To facilitate its manufacturing, this honeycomb structure has been specifically designed with a sequential folding enabling better step-by-step control in a potential production line. From the initial flat shape, the structure

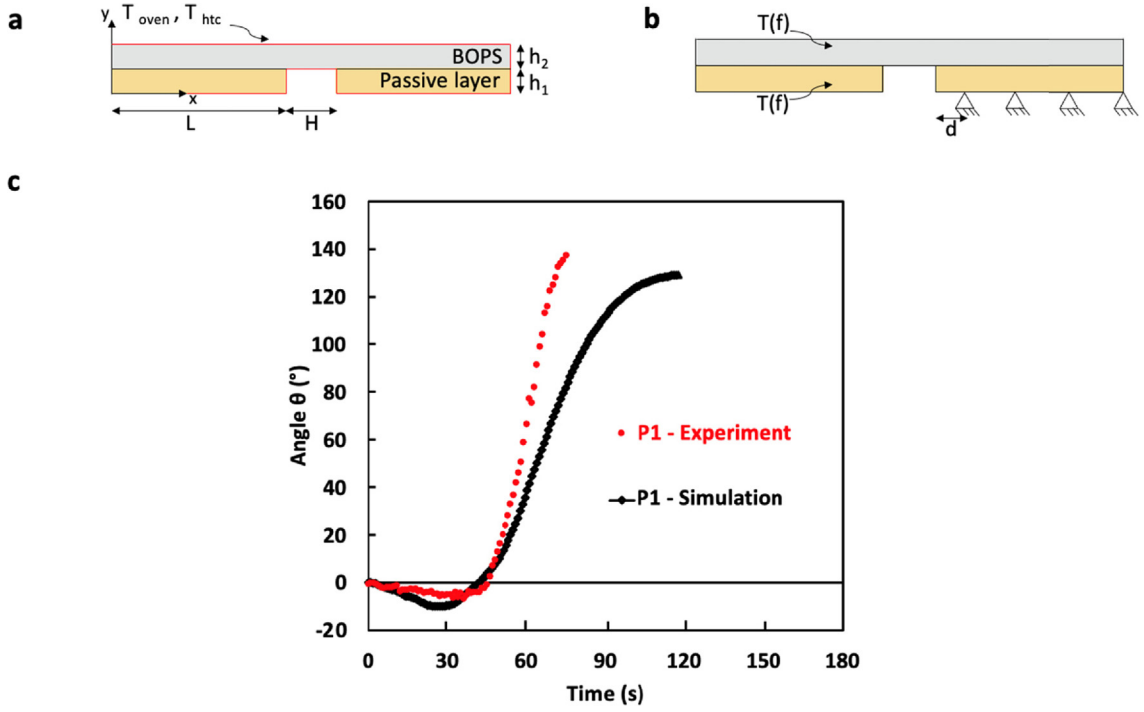

Fig. 2. Finite element method (FEM) analysis. (a) Geometry and boundary conditions of the finite element model to calculate the temperature in the self-folding structure as a function of time, and (b) loads and boundary in the finite element model to predict the time evolution of self-folding. (c) Comparison of experimental data and modelling results of self-folding angles of pattern *P*1 as a function of time.

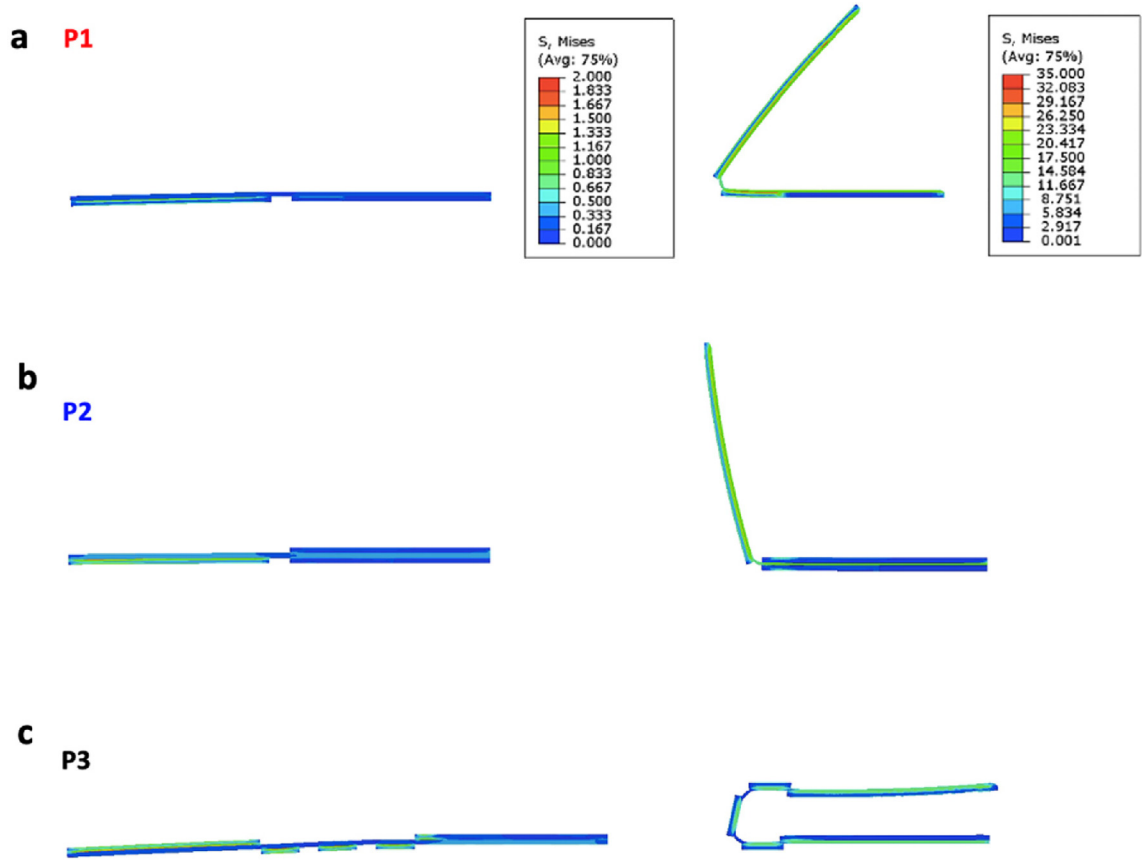

Fig. 3. Finite element method (FEM) analysis. (a-c) Modelling of initial (left) and final angle (right) of patterns *P*1 (a), *P*2 (b) and *P*3 (c) with the local stress values for each modelling.

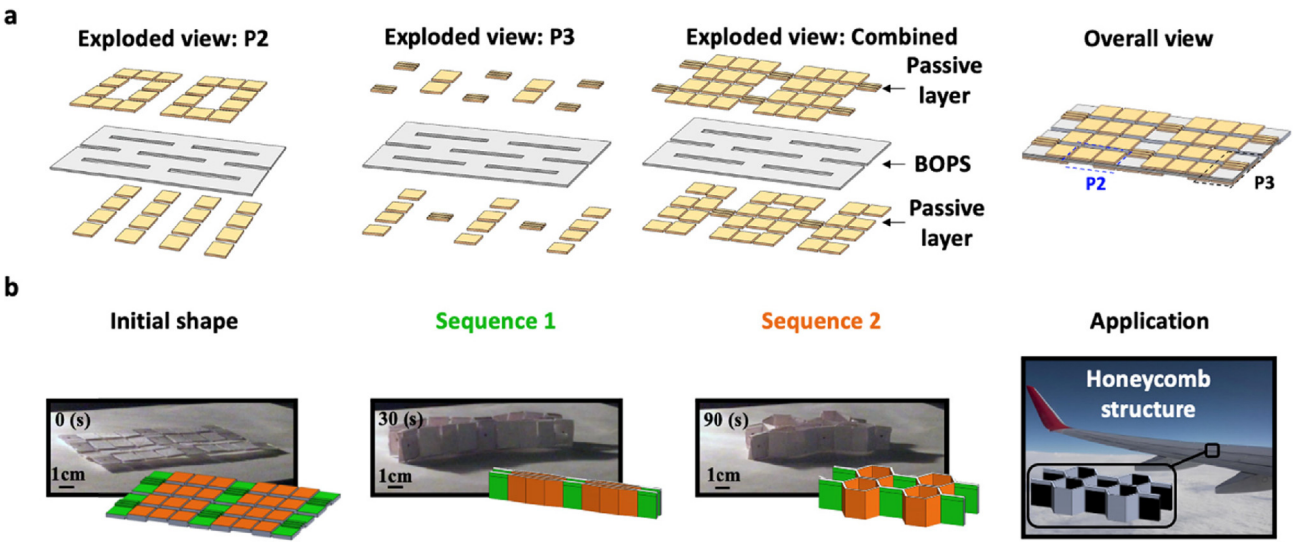

Fig. 4. Sequential self-folding honeycomb structure. (a) Exploded view of the multilayered honeycomb pattern composed of one top layer of passive layer, the BOPS and a bottom layer of passive layer (left), an overall of the honeycomb pattern combining several *P*2 and *P*3 (middle). (b) Images and schematic illustrations of the sequential folding (initial shape, sequence 1 and 2) of a sequential self-folding honeycomb structure with schematic illustrations of their potential applications.

has been developed in such a way with sequence 1 enabling the film to be in a stand-up position. This, in turn, reduces the risk of structural distortions occurring, therefore minimising production time and reducing manufacturing costs. From the stand-up position, sequence 2 can then produce the final structure, with the expansion of the hexagonal honeycomb cells. Such a honeycomb structure is of interest for example in lightweight high bending stiffness structures (Fig. 4b).

It is clear that sequential folding is critical in developing programmable 3D structures and unlocking shapes and functions for multiple applications, which would not be achievable by simultaneous folding.

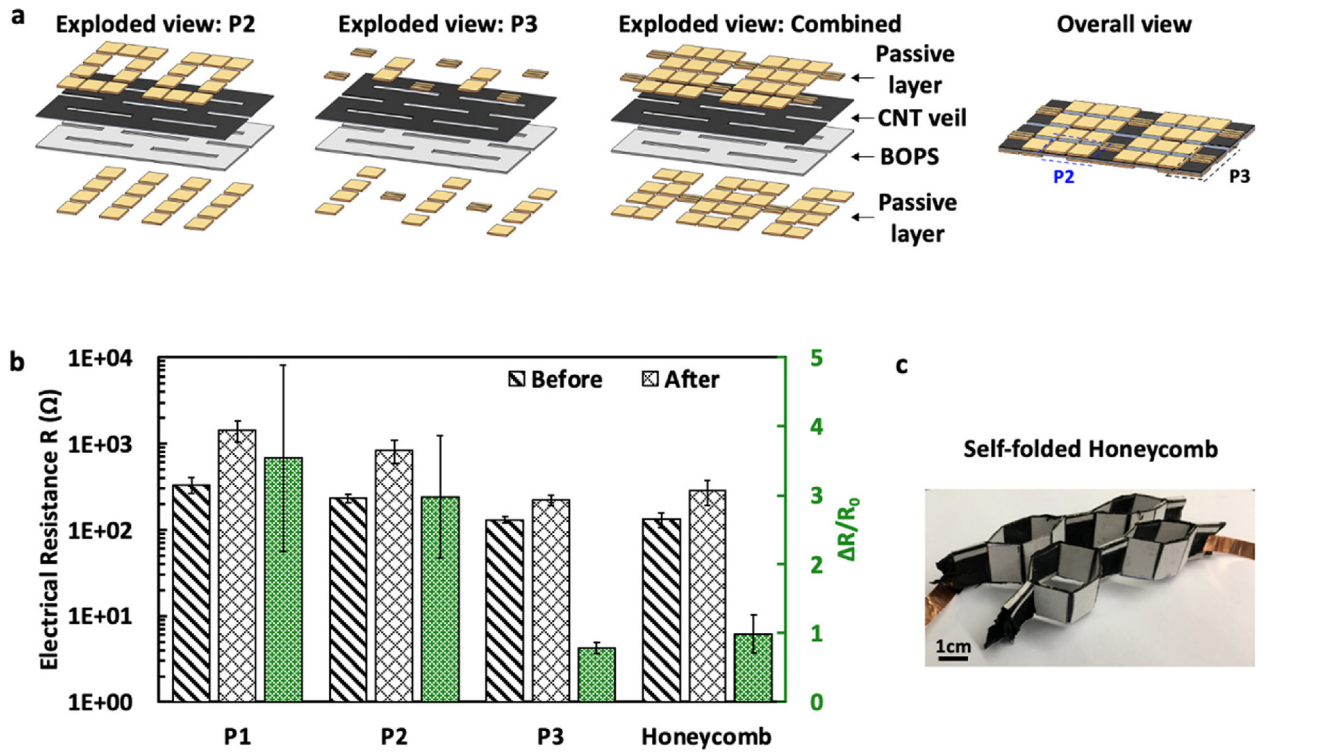

Fig. 5. Self-folding CNTs based honeycomb structure with integrated sensing–actuating functionalities. (a) Exploded view of the multilayered honeycomb pattern composed of one top layer of passive layer, the CNT veil, the BOPS and a bottom layer of passive layer (left), an overall of the honeycomb pattern combining several *P*2 and *P*3 (middle) and the self-folded CNT based honeycomb with 2 electrodes at the diagonally opposite edges of the pattern (right). (b) Electrical resistance of the different patterns *P*1, *P*2, *P*3 and the honeycomb structure, before and after self-folding and $\Delta R/R_0$.

4.4. Multifunctional CNTs sensing self-folded honeycomb structure

Having shown the use of sequential folding to create complex 3D structures, the aim is to demonstrate how bespoke physical properties and functions can also be incorporated. The simple strategy that is proposed herein is the addition of a new ultra-thin functional layer to the patterns studied before, without interfering with the folding kinematics. The functional layer studied herein is a CNT veil. CNT veils exhibit high electrical and thermal conductivity, high fracture energy and high specific surface area [28]. The electrical, thermal and mechanical properties of CNT veils can be orders of magnitude higher than thin depositions of CNTs or graphene [29] or traditional interleaves [30] that, combined with their high bending flexibility [31], makes it an ideal material of choice.

A CNT veil (3–4 μm thick), manufactured by floating catalyst based chemical vapor deposition (FCCVD) method, is interleafed between the paperboard and the BOPS in *P*1, *P*2 and *P*3, as previously explained. When exposed to the same thermal profile as before, all patterns are actuated in a very similar manner, irrespective of the presence of the CNT veil. A self-folded hexagonal honeycomb structure is also demonstrated (Fig. 5a) by combining patterns *P*2 and *P*3.

The CNT-functionalised honeycomb possesses through-the-thickness properties (e.g. electrical and thermal conductivity, Figure S4, SI) at par with in-plane (pre-folding) properties. This is very unusual for composites materials where out-of-plane properties (e.g. mechanical, electrical and thermal) are always and significantly inferior to the in-plane counterparts. But this at first look surprising result can simply be understood by the bespoke 3D orientation of the CNT veil. From this perspective, the actuation mechanism described herein can be seen as a way, for the first time, to accurately position nanoparticles in 3D space and time and, by doing so, controlling properties and anisotropies. Moreover, the actuation mechanism is, in principle, size independent. This means that the nanoparticles 3D positioning is only limited by the accuracy with which 2D patterns can be manufactured. Furthermore, the actuation stimulus does not have to be limited to an external heat source. In our case, for instance, the presence of a conductive CNT layer offers an alternative way of actuating the self-folding: by Joule heating (Figure S5). Sequential folding is possible using strategically located electrodes on the hinges in order to provide a better control of the folded shapes and avoiding folding collisions, thus enabling more complex structures.

It can be observed that there is a small variation of the electrical resistance of the CNT-functionalised honeycomb between the initial 2D shape and the final 3D shape. This can be understood in terms of local deformation that the CNT veil experiences during bending.

For instance, the electrical resistance of CNTs veil composites has been measured before and after folding at an actuation temperature of 140 °C until reaching a maximum folding angle for *P*1, *P*2 and *P*3 of, respectively, 150°, 80° and 190°. After folding, the CNT veil-based composite shows a resistance increasing of about 431 % for *P*1, 360 % for *P*2 and 170 % for *P*3 (Fig. 5b and Figure S6, SI). This is very interesting as the change in resistance can be used to monitor and sense the self-folding during actuation, while it is renownedly difficult to have both sensing and actuation.

5. Conclusions

This paper demonstrates a facile approach to achieve and control sequential folding of 3D structures by designing and combining several simple actuating multilayer units, obtained by combining constraining (passive) layers onto an oriented (active) polymer film. A systematic experimental study was performed to

investigate the mechanisms of self-folding of these multilayer structures, which have been successfully validated by a finite element method (FEM) model able to predict the folding kinematic. The possibility of incorporating multiple patterns into one single piece of shape-programmable structure was also demonstrated.

For the first time, a multifunctional self-folded honeycomb structure, inspired by kirigami, was developed with high out-of-plane electrical and thermal conductivity and with folding sensing ability ($\Delta R/R_0$ = 100–300 %) during the actuation. This development allows to accurately position nanoparticles in 3D space and time and, hence, to control properties and anisotropies, which opens up opportunities for various applications such self-folded structural composite modules as high-power output energy harvester thermoelectric (TE) and high conductivity thermal interfaces.

Overall, incorporating CNTs veil into 3D shape programming enabled a host of multifunctionalities into the structures such as high electrical and thermal conductivity, folding sensing as well as alternative methods to actuate the initial flat active multilayers using Joule heating effect for sequential and accurate folding.

Data availability

Data will be made available on request.

Declaration of Competing Interest

The authors declare that they have no known competing financial interests or personal relationships that could have appeared to influence the work reported in this paper.

Appendix A. Supplementary data

Supplementary data to this article can be found online at https://doi.org/10.1016/j.matdes.2022.111335.

References

[1] Leong, Timothy G et al. "Tetherless thermobiochemically actuated microgrippers." Proceedings of the National Academy of Sciences of the United States of America vol. 106,3 (2009): 703-8. doi:10.1073/pnas.0807698106.

[2] S. Felton et al., A method for building self-folding machines, Science 345 (6197) (2014) 644–646.

[3] S.M. Felton et al., Self-folding with shape memory composites, Soft Matter 9 (32) (2013) 7688–7694.

[4] Zirbel, Shannon A., et al. "Hanaflex: a large solar array for space applications." Micro-and Nanotechnology Sensors, Systems, and Applications VII. Vol. 9467. International Society for Optics and Photonics, 2015.

[5] J. Wu, C. Yuan, Z. Ding, M. Isakov, Y. Mao, T. Wang, H.J. Qi, Multi-shape active composites by 3D printing of digital shape memory polymers, Scientific reports 6 (1) (2016) 1–11.

[6] J.H. Lee, J.C. Choi, S. Won, J.W. Lee, J.G. Lee, H.R. Kim, J.J. Wie, Light-driven complex 3D shape morphing of glassy polymers by resolving spatio-temporal stress confliction, Scientific reports 10 (1) (2020) 1–12.

[7] L. Huang, R. Jiang, J. Wu, J. Song, H. Bai, B. Li, T. Xie, Ultrafast digital printing toward 4D shape changing materials, Advanced materials 29 (7) (2017) 1605390.

[8] M. Shojaeifard, S. Niroumandi, M. Baghani, Programmable self-folding of trilayer and bilayer-hinge structures by time-dependent swelling of tough hydrogels, Journal of Intelligent Material Systems and Structures 1045389X221077435 (2022).

[9] M. Barnes, S.M. Sajadi, S. Parekh, M.M. Rahman, P.M. Ajayan, R. Verduzco, Reactive 3D printing of shape-programmable liquid crystal elastomer actuators, ACS applied materials & interfaces 12 (25) (2020) 28692–28699.

[10] J.M. Boothby, T.H. Ware, Dual-responsive, shape-switching bilayers enabled by liquid crystal elastomers, Soft Matter 13 (24) (2017) 4349–4356.

[11] G. Stoychev et al., Self-folding all-polymer thermoresponsive microcapsules, Soft Matter 7 (2011) 3277–3279.

[12] A. Ta et al., Fabrication of Temperature-Responsive Bending Hydrogels with a Nanostructured Gradient, Adv. Mater. 20 (2008) 2080–2083.

[13] Y. Liu et al., Self-folding of polymer sheets using local light absorption, Soft Matter 8 (2012) 1764–1769.

[14] J. Kim et al., Thermally responsive rolling of thin gel strips with discrete variations in swelling, Soft Matter 8 (2012) 2375–2381.

[15] J. Kim et al., Designing responsive buckled surfaces by halftone gel lithography, Science 335 (6073) (2012) 1201–1205.

[16] T. Chen et al., A "writing" strategy for shape transition with infinitely adjustable shaping sequences and in situ tunable 3D structures, Materials Horizons 3 (6) (2016) 581–587.

[17] Y. Sun et al., Controlled buckling of semiconductor nanoribbons for stretchable electronics, Nature nanotechnology 1 (3) (2006) 201–207.

[18] R. Pelrine et al., High-speed electrically actuated elastomers with strain greater than 100%, Science 287 (5454) (2000) 836–839.

[19] A.A. Deleo et al., Origami-based deployable structures made of carbon fiber reinforced polymer composites, Composites Science and Technology 191 (2020) 108060.

[20] J.-H. Na et al., Programming reversibly self-folding origami with micropatterned photo-crosslinkable polymer trilayers, Advanced Materials 27 (1) (2015) 79–85.

[21] D. Davis et al., "Self-folding of polymer sheets using microwaves and graphene ink." Rsc, Advances 5 (108) (2015) 89254–89261.

[22] E. D'Elia et al., "Electrically-responsive graphene-based shape-memory composites". Applied, Materials Today 15 (2019) 185–191.

[23] J. Mu et al., Origami-inspired active graphene-based paper for programmable instant self-folding walking devices, Science advances 1 (10) (2015) e1500533.

[24] J.G. Lee et al., Multifunctional Three-Dimensional Curvilinear Self-Folding of Glassy Polymers, Journal of Micro-and Nano-Manufacturing 8 (3) (2020) 031004.

[25] X. Xu et al., In-situ curing of glass fiber reinforced polymer composites via resistive heating of carbon nanotube films, Composites Science and Technology 149 (2017) 20–27.

[26] M. Trznadel, M. Kryszewski, Thermal shrinkage of oriented polymers, Journal of Macromolecular Science, Part C: Polymer Reviews 32 (3-4) (1992) 259–300.

[27] C.L. Choy et al., Negative thermal expansion in oriented crystalline polymers, Journal of Polymer Science: Polymer Physics Edition 19 (2) (1981) 335–352.

[28] Y. Ou, C. González, J.J. Vilatela, Understanding interlaminar toughening of unidirectional CFRP laminates with carbon nanotube veils, Composites Part B: Engineering 201 (2020) 108372.

[29] A. Kernin et al., The effect of graphene network formation on the electrical, mechanical, and multifunctional properties of graphene/epoxy nanocomposites, Composites Science and Technology 169 (2019) 224–231.

[30] H. Xu et al., Mechanical and electrical properties of laminated composites containing continuous carbon nanotube film interleaves, Composites Science and Technology 127 (2016) 113–118.

[31] J.W. Kim, J.S. Lee, Influence of interleaved films on the mechanical properties of carbon fiber fabric/polypropylene thermoplastic composites, Materials 9 (5) (2016) 344.